Computer Aided Geometric Design 35–36 (2015) 243–254

Contents lists available at ScienceDirect

Computer Aided Geometric Design

www.elsevier.com/locate/cagd

Smooth bijective maps between arbitrary planar polygons

Teseo Schneider, Kai Hormann *

Università della Svizzera italiana, Lugano, Switzerland

ARTICLE INFO

Article history:
Received 21 February 2015
Accepted 11 March 2015
Available online 24 March 2015

Keywords:
Bijective maps
Harmonic maps

ABSTRACT

Mapping from one planar polygonal domain to another is a fundamental problem in computer graphics and geometric modelling. Exploiting the properties of harmonic maps, we define smooth and bijective maps with prescribed behaviour along the domain boundary. These maps can be approximated in different ways, and we discuss the respective advantages and disadvantages. We further present a simple procedure for reducing their distortion and demonstrate the effectiveness of our approach by providing examples of applications in image warping and surface cross-parameterization. Moreover, we briefly discuss the extension of our construction to 3D and its application to volumetric shape deformation.

1. Introduction

Many applications in computer graphics and geometric modelling require constructing a *smooth* map $f: \Omega_0 \to \Omega_1$ between a *source polygon* $\Omega_0 \subset \mathbb{R}^2$ with n *source vertices* $v_1^0, \dots, v_n^0$ and a *target polygon* $\Omega_1 \subset \mathbb{R}^2$ with the same number of *target vertices* $v_1^1, \dots, v_n^1$, and f should have certain properties.

Bijectivity of f prevents fold-overs, which cause undesirable artefacts in almost all applications. Moreover, it is a necessary requirement for having *symmetry*, in the sense that the construction should give f^{-1} as the mapping from Ω_1 to Ω_0, which in turn allows the user to "undo" a map in an interactive application. It is further desirable that f has a specific *boundary behaviour* and maps each source edge to the corresponding target edge, which implies interpolation at the vertices. Finally, f should have *low distortion*, so that metric quantities measured in Ω_0 are close to those measured in Ω_1.

1.1. Related work

One of the applications of such mappings is image warping, but despite the vast literature on this topic, most approaches cannot guarantee all the requirements stated above. Smooth deformation methods based on radial basis functions (Arad et al., 1994), B-splines (Lee et al., 1997), or biharmonic weights (Jacobson et al., 2011) are not necessarily bijective, so that the target image may exhibit artefacts resulting from fold-overs. Conformal maps (Weber et al., 2009; Weber and Gotsman, 2010), as well as recent techniques based on the minimization of some deformation energy (Poranne and Lipman, 2014) guarantee bijectivity, but do not possess the desired boundary behaviour.

Surface parameterization methods (Floater and Hormann, 2005; Sheffer et al., 2006) can be used to create bijective maps that are piecewise linear along the boundary by interpreting Ω_0 as a (planar) mesh and parameterizing it over the domain Ω_1. However, they require triangulating Ω_0 and provide only piecewise linear solutions (Weber and Zorin, 2014). The same

* Corresponding author.
E-mail address: kai.hormann@usi.ch (K. Hormann).

http://dx.doi.org/10.1016/j.cagd.2015.03.010

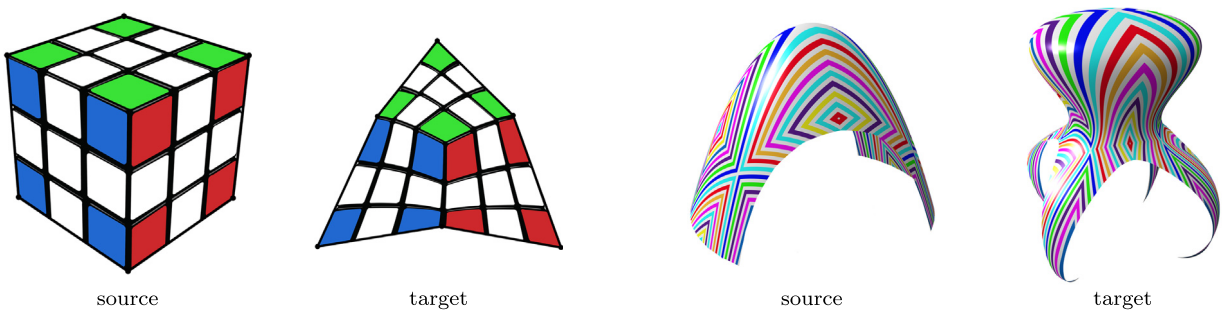

Fig. 1. Smooth bijective maps between polygons (left) and parametric surface patches (right).

restriction holds for quasi-conformal maps (Weber et al., 2012) and variational methods that minimize the distortion of the map (Aigerman et al., 2014; Lipman, 2012; Schüller et al., 2013).

Barycentric mappings (Hormann and Floater, 2006; Weber et al., 2011) naturally provide smooth solutions with piecewise linear boundary behaviour, but they are not necessarily bijective. This limitation can be overcome by introducing a set of intermediate polygons and defining composite barycentric mappings (Schneider et al., 2013), but the overall construction is not symmetric and the derivatives of the mapping are tedious to compute. Another option is to restrict the set of possible domains. Wachspress mappings are known to be bijective as long as both the source and the target polygon are convex (Floater and Kosinka, 2010), and barycentric mappings based on harmonic coordinates (Joshi et al., 2007) are bijective as long as the target polygon is convex. The latter is not surprising, once we notice that they are in fact *harmonic maps* and hence bijective as a consequence of the Radó–Kneser–Choquet theorem (Choquet, 1945; Kneser, 1926; Radó, 1926).

1.2. Contribution

In this paper, we propose to combine two harmonic maps to define a smooth and bijective map between two arbitrary planar polygons (Section 2). This construction is symmetric, and the maps can be approximated in different ways (Section 3), each with its own pros and cons. The different implementations provide a high degree of flexibility, ranging from an efficient computation to exact pointwise evaluation. While these methods are guaranteed to generate bijective maps only in the limit, as they converge to the exact solution, our experiments show that they produce bijective results in practice.

The behaviour of the map along the boundary can be prescribed (for example, to be piecewise linear), giving the user an intuitive way of controlling the map in applications such as image warping and surface cross-parametrization (see Fig. 1). Moreover, the distortion appears to be lower compared to previous work (Section 4).

The simplicity of our construction allows for several extensions (Section 5), including a simple non-linear optimization procedure to reduce the distortion of the map without compromising the other properties and a strategy which appears to give almost conformal results. Moreover, our method trivially extends to smooth volumetric maps between polyhedral domains, and although the theoretical guarantees on bijectivity are lost (Laugesen, 1996), our experiments demonstrate that the maps are bijective even for non-trivial examples.

Our contributions can be summarized as follows:

- We propose a symmetric construction for defining smooth and bijective maps between two arbitrary polygonal domains with prescribed boundary behaviour.
- We compare and analyse in depth three numerical strategies for approximating these bijective maps.
- We describe a simple optimization strategy for decreasing the distortion of the map.
- We present some results on the extension of our method to the volumetric setting.

2. Smooth bijective maps

Given two planar domains Ω, Ω' and a bijective boundary mapping $b\colon \partial\Omega \to \partial\Omega'$, the unique map $\varphi\colon \Omega \to \Omega'$ that solves the Laplace equation

$$\Delta\varphi = 0 \tag{1a}$$

subject to the continuous Dirichlet boundary condition

$$\varphi|_{\partial\Omega} = b \tag{1b}$$

is called a *harmonic map*. The map φ is smooth, and it follows from the Radó–Kneser–Choquet theorem that φ is bijective if Ω' is convex.

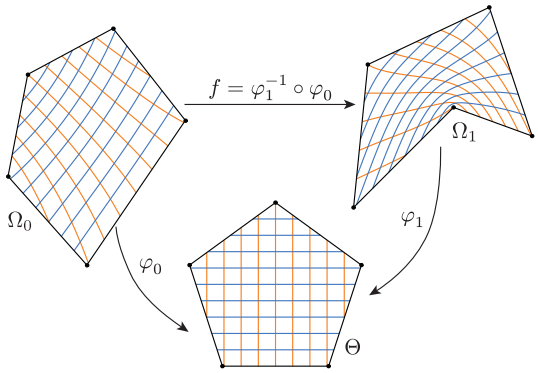

Fig. 2. Main idea for defining smooth bijective maps.

In order to define the smooth bijective map f between Ω_0 and Ω_1, we simply introduce an intermediate convex polygon Θ with n vertices, combine the two harmonic maps $\varphi_0 \colon \Omega_0 \to \Theta$ and $\varphi_1 \colon \Omega_1 \to \Theta$ as shown in Fig. 2, and let

$$f = \varphi_1^{-1} \circ \varphi_0. \tag{2}$$

For simplicity, we can use a regular n-gon as Θ and piecewise linear boundary constraints b_0 and b_1, but it is possible to deviate from these default choices (Sections 5.1 and 5.2).

The concept of constructing bijective maps in this way has already been used in the context of mesh parameterization (Weber and Zorin, 2014), mesh morphing (Kanai et al., 1997), and surface correspondences (Lipman and Funkhouser, 2009), but only in the discrete setting. Instead, we consider smooth maps, and we also discuss several extensions (Section 5).

3. Implementation

The approach described in Section 2 poses two practical challenges. First, we need to solve the boundary value problem (1), and the exact solution is known only for simple domains like rectangles. However, an approximate solution can be computed in different ways (Section 3.1). Second, we have to invert the map φ_1, and again we treat this problem numerically (Section 3.2).

3.1. Solving the Laplace equation

There are three main methods for solving the Laplace equation: the *finite element method* (FEM) (Strang and Fix, 2008), the *boundary element method* (BEM) (Hall, 1994; Rustamov, 2007), and the *method of fundamental solutions* (MFS) (Fairweather and Karageorghis, 1998; Martin et al., 2008). Each method comes with certain advantages and disadvantages. Since these methods are designed to find *harmonic functions* $\varphi \colon \Omega \to \mathbb{R}$, we apply them to both components of our harmonic maps φ_0, φ_1 separately.

3.1.1. Finite element method

By calculus of variations, φ solves (1a), if and only if

$$\int_\Omega \Delta\varphi \, \psi = 0 \tag{3}$$

for a certain set of *test functions* ψ. In the finite element approach this set contains all functions that vanish on the boundary of Ω. Using this fact and integration by parts, the weak form (3) can be rewritten as

$$\int_\Omega \nabla\varphi \, \nabla\psi = 0. \tag{4}$$

In our implementation, we consider the space of piecewise linear functions over a constrained Delaunay triangulation of Ω, spanned by the hat functions $B_1, \ldots, B_m \colon \Omega \to \mathbb{R}$, and the approximation $\sum_{i=1}^m c_i B_i$ of φ. Assuming that the first $k < m$ basis functions correspond to the interior nodes and thus vanish at the boundary, the weak form (4) becomes

$$\sum_{i=1}^m c_i \int_\Omega \nabla B_i \nabla B_j = 0, \qquad j = 1 \ldots, k.$$

The coefficients $c_{k+1}, \ldots, c_m$ are given by the boundary condition (1b), and the others can be found by solving a sparse linear system of size k, where the off-diagonal elements are the well-known *cotangent weights* (Eck et al., 1995; Pinkall and Polthier, 1993; Strang and Fix, 2008).

Fig. 3. Nodes used by BEM (left) and nodes and sites used by MFS (right).

3.1.2. Boundary element method

The principal idea of the boundary element method is to first solve a small problem on the boundary and then extend this solution to the interior. To this end, we use the divergence theorem to rewrite (3) as

$$\int_{\partial\Omega} \frac{\partial\varphi}{\partial n}\,\psi - \int_{\Omega} \nabla\varphi\,\nabla\psi = 0$$

and then apply integration by parts to the last term to obtain

$$\int_{\partial\Omega} \frac{\partial\varphi}{\partial n}\psi - \int_{\partial\Omega} \frac{\partial\psi}{\partial n}\varphi + \int_{\Omega} \varphi\,\Delta\psi = 0,$$

where n is the unit normal to $\partial\Omega$. In the boundary element approach, the set of test functions is $\{G_x : x \in \Omega\}$, where

$$G_x(y) = -\frac{1}{2\pi}\log(\|x-y\|) \tag{5}$$

are 2D Green's functions. Since $\Delta G_x(y) = \delta(x-y)$, we obtain the *boundary integral equation*

$$\int_{\partial\Omega} \frac{\partial\varphi}{\partial n} G_x - \int_{\partial\Omega} \frac{\partial G_x}{\partial n}\varphi + \omega(x)\varphi(x) = 0, \qquad x \in \Omega, \tag{6}$$

where

$$\omega(x) = \begin{cases} \frac{\alpha(x)}{2\pi}, & \text{for } x \in \partial\Omega, \\ 1, & \text{otherwise,} \end{cases}$$

with $\alpha(x)$ denoting the exterior angle at $x \in \partial\Omega$, that is, $\alpha(x) = \pi$ along the open edges of Ω.

In our implementation, we sample the boundary of Ω with the *nodes* $x_1, \dots, x_m$, which include the vertices v_i (see Fig. 3), and consider the corresponding space of piecewise linear functions, spanned by the one-dimensional hat functions $B_1, \dots, B_m \colon \partial\Omega \to \mathbb{R}$. This allows us to use

$$\varphi(x) = \sum_{i=1}^{m} c_i B_i(x), \qquad \frac{\partial\varphi}{\partial n}(x) \approx \sum_{i=1}^{m} d_i B_i(x)$$

for all $x \in \partial\Omega$, so that (6), evaluated at x_j, turns into

$$\sum_{i=1}^{m} d_i \int_{\partial\Omega} B_i G_{x_j} \approx \sum_{i=1}^{m} c_i \left(\int_{\partial\Omega} \frac{\partial G_{x_j}}{\partial n} B_i + \omega(x_j) B_i(x_j) \right)$$

for $j = 1, \dots, m$. Since the c_i are given by the boundary condition (1b), we then determine the coefficients d_i by solving a dense linear system of size m. After solving this small system on the boundary, we are ready to evaluate φ at any $x \in \Omega$ by rearranging (6),

$$\varphi(x) \approx \frac{1}{\omega(x)} \sum_{i=1}^{m} \left(d_i \int_{\partial\Omega} B_i G_x - c_i \int_{\partial\Omega} \frac{\partial G_x}{\partial n} B_i \right).$$

We employ Gaussian quadrature for evaluating all required boundary integrals numerically, because they do not have closed forms.

3.1.3. Method of fundamental solutions

The main idea of the method of fundamental solutions is to exploit the fact that Green's functions (5) and linear functions are harmonic by construction. We approximate φ by

$$\hat{\varphi} = \sum_{i=1}^{m} w_i\, G_{s_i} + A$$

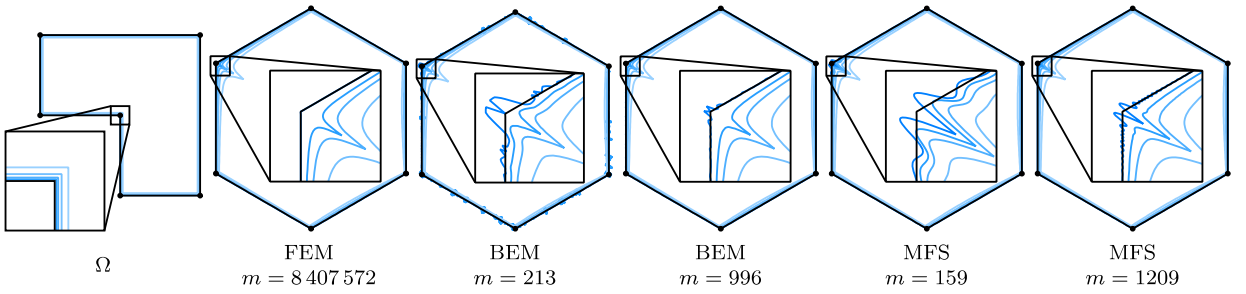

Fig. 4. Behaviour of the different approximations to the harmonic mapping φ from Ω to the regular hexagon Θ near the boundary. The curves correspond to the images of the boundary and boundary offsets at distances 0.001, 0.002, 0.004, and 0.008 (from dark to light), relative to the size of the bounding box of Ω.

for certain *sites* $s_1, \dots, s_m$ (see Fig. 3) and some linear function A. In order to avoid singularities inside the domain Ω, the sites need to be placed outside the polygon, and we follow the strategy of Martin et al. (2008) to determine their positions. The unknown weights w_i and the coefficients of A are then determined by minimizing

$$\sum_{j=1}^{k} |\hat{\varphi}(x_j) - b(x_j)|^2$$

for $k \gg m$ uniformly spaced nodes $x_j \in \partial\Omega$, which can be done by solving a dense over-determined linear system of size $k \times (m+3)$ in the least squares sense.

3.1.4. Comparison

The main advantages of FEM are speed and robustness, but it provides only piecewise linear approximations of the exact solution. Consequently, the first derivatives are constant per triangle and higher derivatives vanish, which is a disadvantage for applications that rely on these quantities being smooth. Another disadvantage is that FEM requires choosing the triangulation a priori, resulting in a fixed resolution of the result. If later a higher resolution is needed, the problem needs to be solved again from scratch. Finally, the result is not guaranteed to be bijective, because the cotangent weights can be negative. Although non-bijectivity usually does not occur in practice, especially at high resolution, it can be prevented by replacing the cotangents with positive weights (Weber and Zorin, 2014). The resulting piecewise linear mapping is then guaranteed to be bijective, but it does no longer approximate the harmonic solution.

The principal benefits of BEM and MFS are that they give smooth closed-form approximations of φ and that derivatives can be computed analytically. For BEM, every function evaluation requires calculating $2m$ boundary integrals, which is rather slow, whereas evaluating the MFS approximation and its derivatives is fast, because they have simple closed forms. The main disadvantage of both methods is that the boundary conditions are not satisfied exactly and hence they do not guarantee to linearly map the edges from source to target polygon. Instead, the image of $\partial\Omega$ can exhibit oscillations, especially near concave corners, as shown in Fig. 4. This effect extends to the interior, but disappears quickly with increasing distance to the boundary. Moreover, these oscillations shrink as we raise the number m of basis functions. In the case of BEM, this behaviour stems from the fact that the normal derivative at the boundary of Ω is only approximated by a piecewise linear function. For MFS, it is a consequence of enforcing the boundary constraints only in a least squares sense and at k discrete nodes.

On a theoretical level, this lack of linear precision along the boundary means that the target domain is not convex, and even though both the BEM and the MFS approximations are harmonic by construction, the Radó–Kneser–Choquet theorem cannot be used to conclude their bijectivity. However, as m increases, both methods converge to the exact harmonic and bijective solution, and so they are bijective for a sufficiently large m. In all our examples we observe that even moderately large values of m (less than 1000) are enough to obtain mappings which are practically bijective, in the sense that the Jacobian is positive at a dense set of sample points. However, BEM is usually more precise near the boundary than MFS and seems to converge faster.

Fig. 5 shows an example of a smooth bijective map and the determinant of its Jacobian, approximated with the different methods. The close-ups confirm that the FEM solution is only piecewise linear, while the others are smooth, and that the MFS solution has artefacts near the boundary due to the oscillations mentioned before. Table 1 summarizes the pros and cons of the methods.

3.2. Inverting φ_1

Inverting the FEM approximation of φ_1 is simple, because it is a piecewise linear map between a Delaunay triangulation of Ω_1 and a corresponding triangulation of Θ. Hence, for any $x \in \Theta$ we search for the triangle T in Θ that contains x using a k-d tree, compute the local coordinates of x with respect to T, and apply them to the corresponding triangle in Ω_1. This gives an approximation of $\varphi_1^{-1}(x)$, where the accuracy depends on the size of T. However, even if the triangles in Ω_1 are

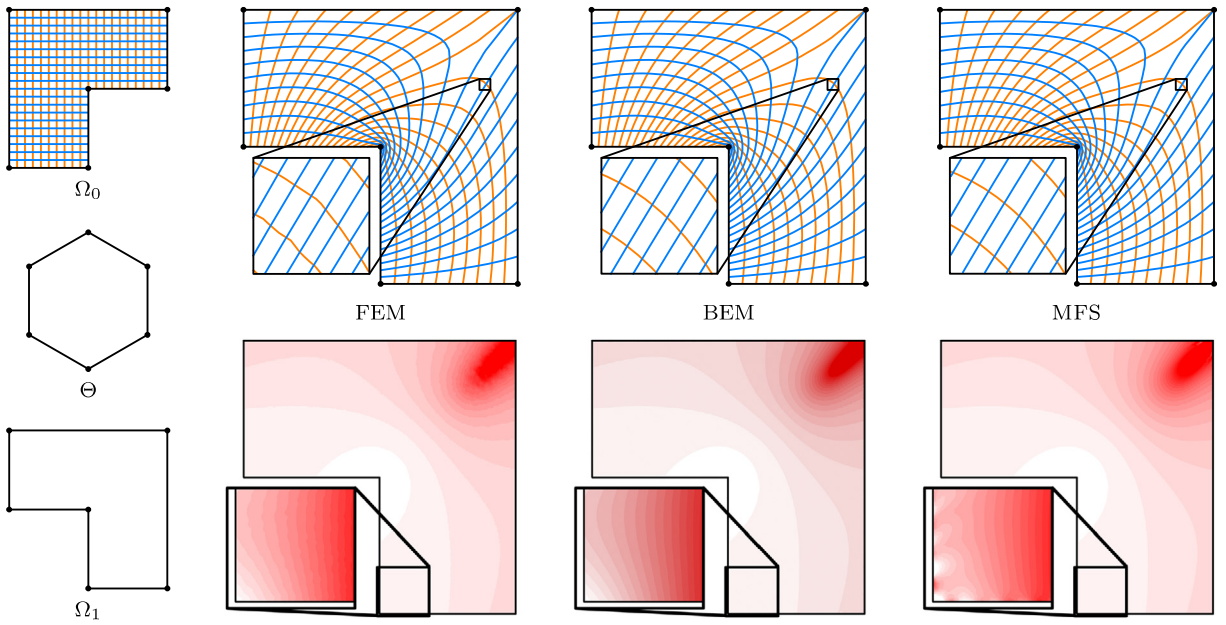

Fig. 5. Comparison between different methods to approximate a smooth bijective map between Ω_0 and Ω_1. The top row visualizes the mapping itself, while the determinant of its Jacobian is colour-coded in the bottom row.

Table 1
Pros and cons of the different methods.

	Smooth	Meshless	Exact on $\partial\Omega$	Precise near $\partial\Omega$	Fast
FEM	×	×	✓	✓	✓
BEM	✓	✓	×	✓	×
MFS	✓	✓	×	×	✓

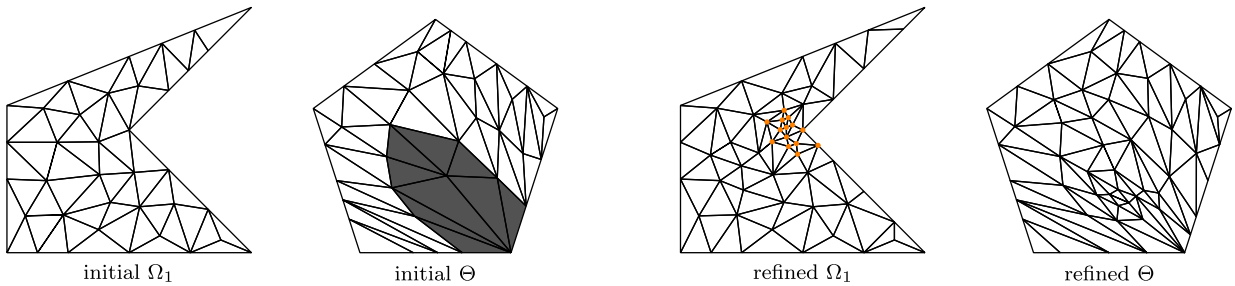

Fig. 6. One step of the adaptive refinement strategy: regions with big triangles in Θ are detected (grey) and the corresponding regions in Ω_1 are refined by inserting new points, so that the big triangles are removed from Θ.

small, their images under φ_1 in Θ can be big and the only way to improve the accuracy is to recompute the approximation of φ_1 with a denser mesh.

For BEM and MFS we can proceed similarly by first triangulating Ω_1 and then mapping the nodes, which induces a triangulation of Θ. Since both methods provide smooth solutions, we can now employ an adaptive refinement strategy that finds all big triangles in Θ, refines the corresponding triangles in Ω_1, and repeats this process until all triangles in Θ are sufficiently small (see Fig. 6), which in practice requires only few steps.

A better option is to exploit the fact that BEM and MFS provide gradients and Hessians of the solution. Hence, we can use efficient numerical solvers to approximate $\varphi_1^{-1}(x)$ more accurately. In our implementation we use *Ipopt* (Wächter and Biegler, 2006) to minimize the function $d(y) = \|x - \varphi_1(y)\|^2$, which is convex and guaranteed to be zero at the optimal solution y^*. This minimization needs to constrain y to the interior of Ω_1, because the harmonic function φ_1 is undefined outside Ω_1. This is no problem for convex domains, but we need to be careful if Ω_1 is concave. In that case we decompose Ω_1 into triangles and constrain the optimization to the triangle T whose image $\varphi_1(T)$ contains x. If the solver finds a minimum at some y with $d(y) > 0$, then we know that the optimal y^* needs to be found in some other triangle. But when

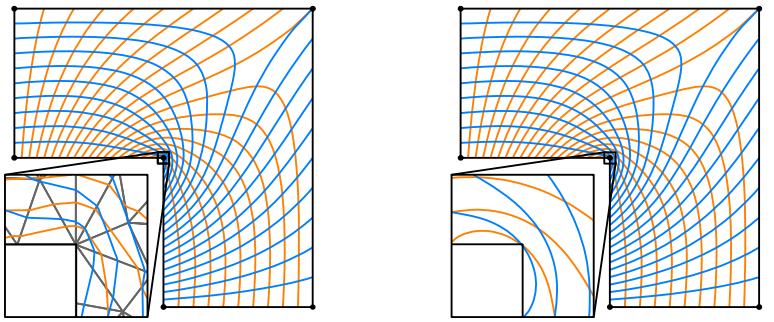

Fig. 7. Inverting φ_1 with a piecewise linear approximation (left) and pointwise minimization (right).

Fig. 8. Deforming a source image (left) with smooth bijective maps (centre) and composite mean value maps (right). The results are globally similar, but our method has less distortion (grey boxes).

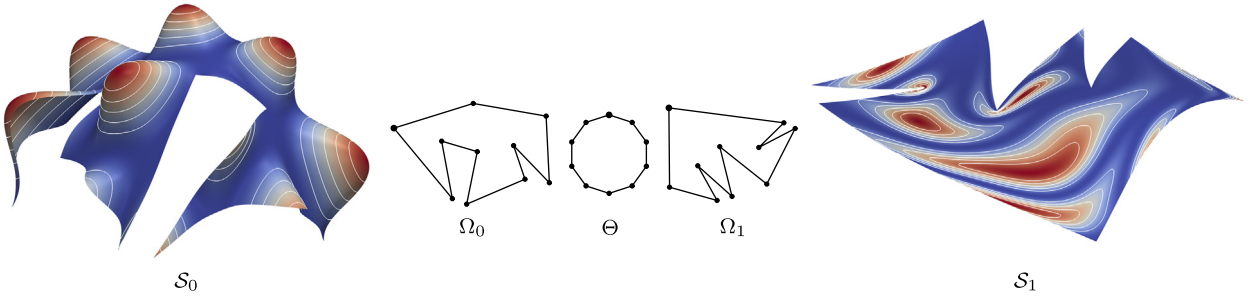

Fig. 9. Using a smooth surface cross-parameterization to transfer a colour-valued signal from $\mathcal{S}_0$ to $\mathcal{S}_1$.

this happens, y lies on one of the edges of T and we keep searching in the neighbouring triangle which shares this edge. However, this approach is much slower, because it requires several evaluations of φ_1 and its derivatives.

Fig. 7 illustrates the results obtained by both inversion procedures. The close-ups clearly show that the first method provides only piecewise linear results, while the result of the second approach is smooth. However, the minimization procedure takes several minutes, whereas the other procedure can be computed in a few seconds.

4. Results

4.1. Image warping

Figs. 1 and 8 show the results of applying smooth bijective maps to deform images. For this application, we use FEM, trading smoothness for speed, because images are discrete and the piecewise linear solution is sufficient if the triangulation density matches the image resolution.

4.2. Surface cross-parameterizations

Another application of our method is the construction of a map between two surface patches $\mathcal{S}_0 : \Omega_0 \to \mathbb{R}^3$ and $\mathcal{S}_1 : \Omega_1 \to \mathbb{R}^3$, which are parameterized over the planar domains Ω_0 and Ω_1, respectively. Such a surface cross-parameterizations $g : \mathcal{S}_0 \to \mathcal{S}_1$ is simply given by

$$g = \mathcal{S}_1^{-1} \circ f \circ \mathcal{S}_0.$$

For this application, we prefer MFS with smooth inverse, because the surface patches are smooth and it is natural to expect the same from the mapping. Moreover, it is faster than BEM, and as long as we are not interested in derivatives, the artefacts near the boundary are negligible. Two examples are shown in Figs. 1 and 9.

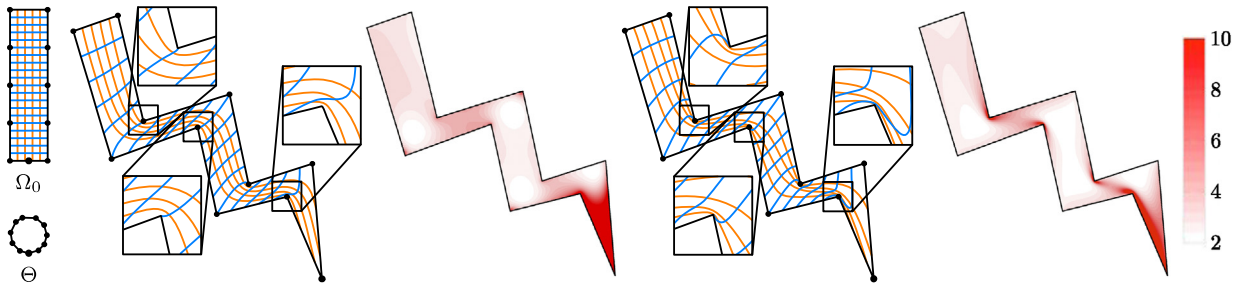

Fig. 10. Comparison of our method (left) with Schneider et al. (2013) (right). The energy plots show the conformal distortion per point, clamped at 10. The overall L_2-distortion of our map is 7.03, compared to 203.77 for Schneider et al. (2013).

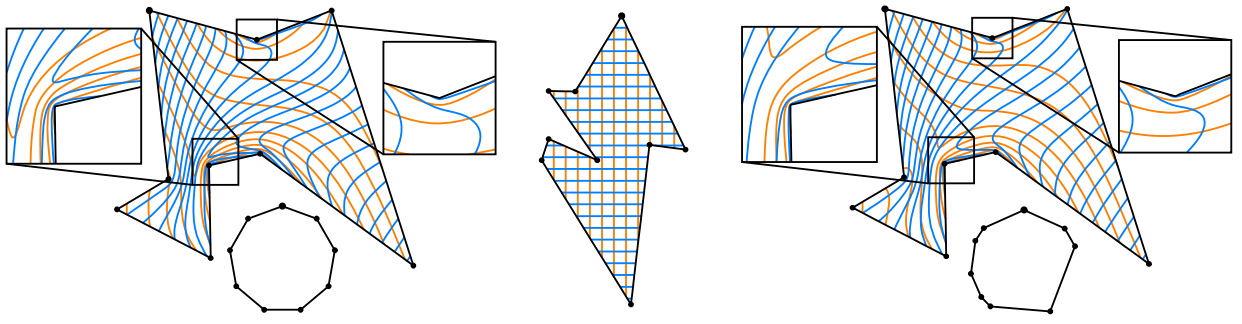

Fig. 11. Effect of mapping from Ω_0 (centre) to Ω_1 using a regular (left) and an irregular (right) intermediate polygon.

4.3. Comparison

To the best of our knowledge, the only other approach for constructing smooth bijective maps is described by Schneider et al. (2013). The example in Fig. 8 suggests that our method gives maps with lower distortion. To support this hypothesis, we measured and compared the actual distortion of both maps.

In Fig. 10 we visualize the *conformal distortion* $\sigma_1/\sigma_2 + \sigma_2/\sigma_1$ (Hormann and Greiner, 2000), where σ_1 and σ_2 are the singular values of the Jacobian of the map. The energy plot and the close-ups illustrate that our map behaves better around the concave corners of the target polygon, and the overall distortion is much lower. A similar behaviour can be observed in Fig. 13, where the *isometric distortion* $\max(\sigma_1, 1/\sigma_2)$ (Sorkine et al., 2002) is considered. We performed similar tests with different polygons and energies, and since the results are all similar, we decided to show only a few prototypical examples.

For these comparisons we use BEM, because it provides the most reliable derivative data, which is needed for computing the distortion.

5. Extensions

5.1. Reducing the distortion

An interesting fact to observe is that the mapping f depends on the shape of Θ, as illustrated in Fig. 11. In this example we compare the result of using a regular polygon versus an irregular cyclic polygon with edge lengths proportional to the average lengths of corresponding source and target edges.

This flexibility can actually be used to reduce the distortion of the map. We implemented a simple strategy, which minimizes a given distortion energy by moving one vertex of Θ at a time under the constraint that Θ remains convex. More specifically, to optimize the position of a vertex v of Θ, we approximate the gradient of the distortion energy with respect to v, using finite differences, resulting in a displacement vector Δv. We then move v to $v + \Delta v$ and check if this new position violates the convexity constraints of Θ. If that is the case, then we iteratively halve Δv until the constraints are met.

An example of this optimization procedure, where we reduce the overall conformal distortion of the map by about 10%, is shown in Fig. 12. A similar improvement can be obtained for the isometric distortion of the map, as illustrated in Fig. 13, which also compares the result to the result by Schneider et al. (2013). Table 2 summarizes the distortions obtained with our method, using regular and optimized intermediate polygons, and with the method proposed by Schneider et al. (2013) for all examples shown in this paper.

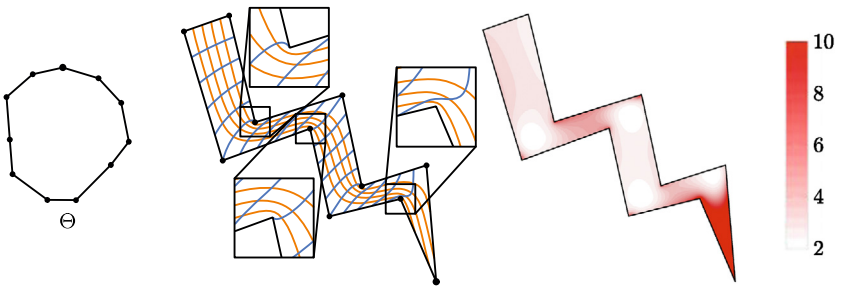

Fig. 12. Optimizing the shape of Θ for the example in Fig. 10 reduces the overall conformal distortion from 7.03 to 6.45.

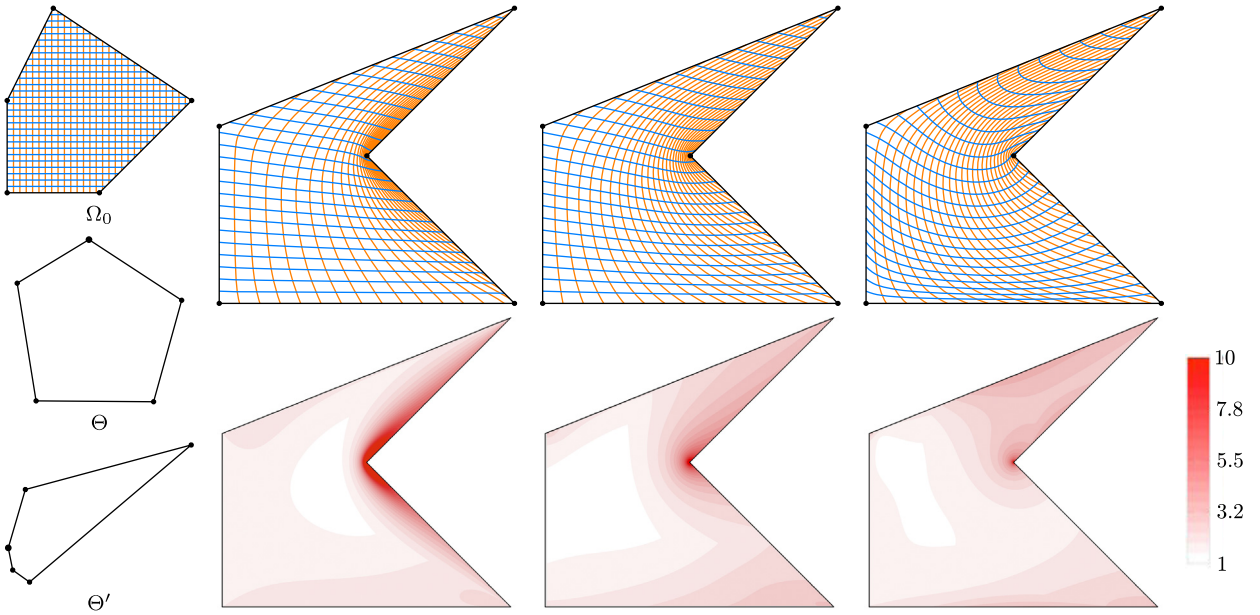

Fig. 13. Comparison of smooth bijective maps generated by Schneider et al. (2013) (left) and our method for an irregular (centre) and the optimized (right) intermediate polygon. The respective overall isometric distortions are 7.34, 3.02, and 2.49.

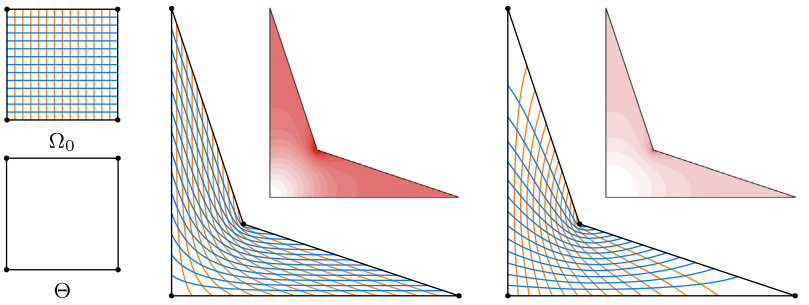

Fig. 14. Effect of changing the behaviour of the boundary conditions for φ_1 from linear (left) to quadratic (right).

5.2. Boundary conditions

Most applications require linearity on the boundary, but with our method we can also impose a different boundary behaviour, similar to how it is suggested by Weber et al. (2011). In the example in Fig. 14 we specify a linear behaviour for the edges of Ω_0 and a quadratic behaviour for the edges of Ω_1. That is, the boundary condition b_1 for any point $p = (1-t)v_1^1 + tv_2^1$ on the edge $[v_1^1, v_2^1]$ of Ω_1 is set to $b_1(p) = (1-t^2)w_1 + t^2 w_2$, where $[w_1, w_2]$ is the corresponding edge of Θ, and similarly for the other edges. This increases the density of the grid lines near the concave as well as the lower left target vertex and also happens to reduce the conformal distortion. It remains future work to exploit this flexibility to further reduce the distortion of the mapping.

Table 2
Average and maximum conformal and isometric distortions for composite mean value maps (Schneider et al., 2013) and our smooth bijective maps based on regular intermediate polygons Θ and optimized polygons Θ'.

Figure	Average distortion						Maximum distortion					
	conformal			isometric			conformal			isometric		
	Schneider et al. (2013)	Θ	Θ'	Schneider et al. (2013)	Θ	Θ'	Schneider et al. (2013)	Θ	Θ'	Schneider et al. (2013)	Θ	Θ'
5	2.93	2.84	2.78	2.85	2.60	2.15	104.86	89.53	75.01	57.53	96.80	83.17
8	2.91	2.85	–	2.10	1.95	–	96.59	96.07	–	88.14	68.61	–
11	7.99	6.41	–	3.63	3.59	–	99.96	99.41	–	99.25	94.30	–
12	203.77	7.03	6.45	232.05	5.57	5.18	107 402	2481.40	1968.75	122 576	1883.76	1679.25
13	9.32	4.85	4.53	7.34	3.02	2.49	99.76	99.86	89.14	99.98	97.79	84.67
14	9.26	6.13	–	8.28	5.02	–	99.61	83.26	–	100.00	82.35	–

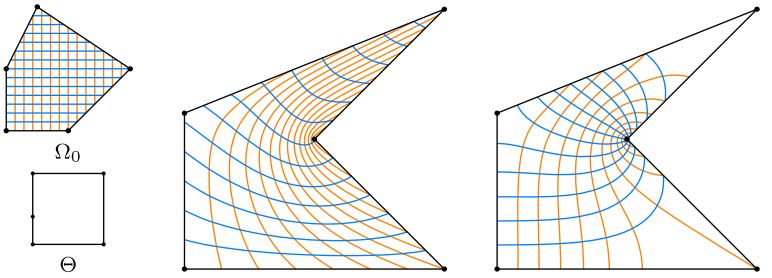

Fig. 15. Effect of replacing Dirichlet boundary conditions (left) with mixed Neumann/Dirichlet boundary conditions (right).

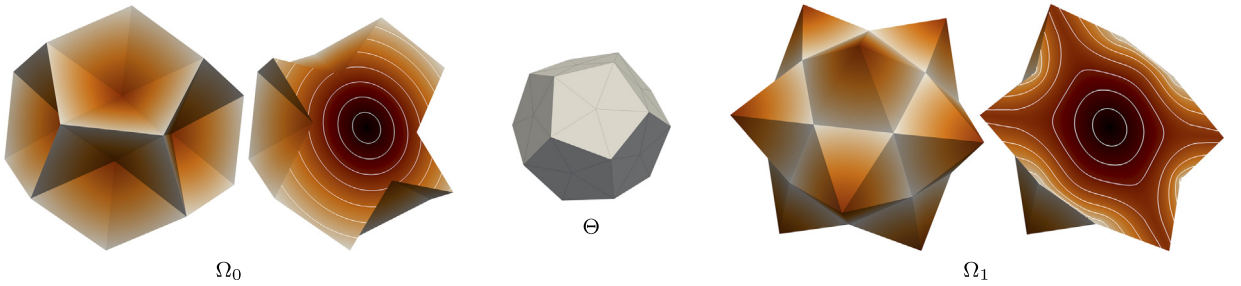

Fig. 16. Using a smooth volumetric mapping to transfer a colour-valued signal from one polyhedron to another.

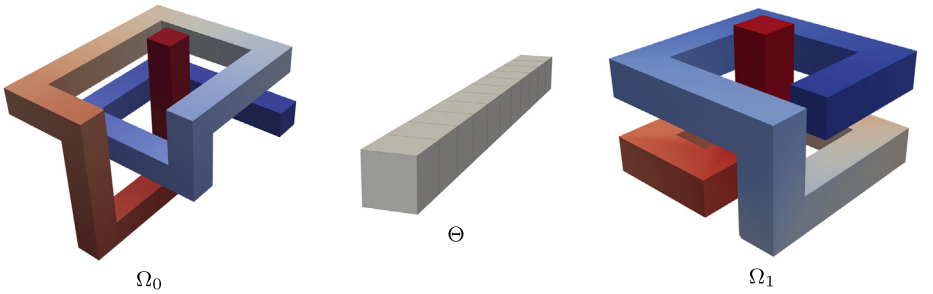

Fig. 17. Smooth volumetric mapping between two polyhedral domains with quadrilateral faces.

Another extension consists of imposing natural boundary conditions, which requires Θ to be the unit square, possibly with side nodes. This particular choice allows us to interpret the components of φ as two coordinate functions $x, y: \Omega \to [0, 1]$. We then solve for x by specifying Dirichlet boundary conditions on the two horizontal and Neumann boundary conditions on the two vertical edges of the unit square and vice versa when solving for y. For the example in Fig. 15, this approach produces more conformal results, but we have not further investigated this behaviour, yet.

5.3. Three dimensional mappings

Our approach easily extends to volumetric mappings between two polyhedral domains in $\mathbb{R}^3$ with the same topology, as shown in Fig. 16. Unfortunately, the Radó–Kneser–Choquet theorem does not hold in $\mathbb{R}^3$, and there is no mathematical guarantee that our mapping is bijective. However, in our experiments we did not observe any problems, and it even works for the rather extreme example in Fig. 17.

6. Conclusions

The smooth maps f between two polygonal domains in (2) satisfy most of the properties requested by common applications in computer graphics and related fields. They are bijective and symmetric, and we can fully control their boundary behaviour. In addition, the construction of f is transitive in the sense that $f_k \circ f_{k-1} \circ \ldots \circ f_1 = g$, where $f_i: \Omega_{i-1} \to \Omega_i$, $i = 1, \ldots, k$ and $g: \Omega_0 \to \Omega_k$. This guarantees an intuitive behaviour in an interactive image warping application where the user modifies an image in several steps by moving the vertices of the control polygon. The transitivity then assures that the result is independent of the way and the order in which the vertices are moved to arrive at the target positions. Moreover, if the user moves the vertices back to their initial positions, the image will be restored, because g will be the identity.

While the smooth maps from Section 2 remain theoretical for now, unless in a few simple cases where closed form solutions of harmonic maps are known, we present and compare three approximation methods in Section 3. In a nutshell, FEM is the method of choice for visualization purposes and other applications where only a fixed resolution and no derivative values are required. BEM and MFS are instead preferable for numerical simulations and other applications that require continuous derivatives of the mapping. Among the two, MFS is considerably faster, but BEM provides more reliable values close to the boundary of the domain. Hence, in applications like image warping, where the interpolation property on the boundary is not essential, a reasonable guideline is to make sure that some minimal distance is kept between the image and the surrounding polygon, so that the deformation can be computed faithfully and efficiently with MFS.

A limitation of our method is that we cannot provide any bounds on the distortion of the maps, even though we describe how to reduce it. Compared with state-of-the-art methods for generating piecewise linear bijective maps, our results usually have a higher distortion, because the optimization is limited by the rigidity of the harmonic functions φ_0 and φ_1. But compared to the only other method that we are aware of for computing smooth bijective maps (Schneider et al., 2013), our maps usually have considerably lower distortion.

An advantage of our approach is its simplicity, which allows it to be extended in several ways. While we have only touched on this versatility and reported some preliminary results, it remains future work to fully explore and understand these extensions.

Acknowledgements

We thank the anonymous reviewers for their insightful comments, and Daniele Panozzo and Olga Sorkine-Hornung for useful discussions and technical assistance. This work was supported by the SNF under project number 200020_156178.

References

Aigerman, N., Poranne, R., Lipman, Y., 2014. Lifted bijections for low distortion surface mappings. ACM Trans. Graph. 33 (4). Article 69, 12 pp.
Arad, N., Dyn, N., Reisfeld, D., Yeshurun, Y., 1994. Image warping by radial basis functions: application to facial expressions. CVGIP: Graph. Models Image Process. 56 (2), 161–172.
Choquet, G., 1945. Sur un type de transformation analytique généralisant la représentation conforme et définie au moyen de fonctions harmoniques. Bull. Sci. Math. 69, 156–165.
Eck, M., DeRose, T., Duchamp, T., Hoppe, H., Lounsbery, M., Stuetzle, W., 1995. Multiresolution analysis of arbitrary meshes. In: Proceedings of SIGGRAPH. Los Angeles, pp. 173–182.
Fairweather, G., Karageorghis, A., 1998. The method of fundamental solutions for elliptic boundary value problems. Adv. Comput. Math. 9 (1–2), 69–95.
Floater, M.S., Hormann, K., 2005. Surface parameterization: a tutorial and survey. In: Dodgson, N.A., Floater, M.S., Sabin, M.A. (Eds.), Advances in Multiresolution for Geometric Modelling. Springer, Berlin, Heidelberg, pp. 157–186.
Floater, M.S., Kosinka, J., 2010. On the injectivity of Wachspress and mean value mappings between convex polygons. Adv. Comput. Math. 32 (2), 163–174.
Hall, W.S., 1994. The Boundary Element Method. Solid Mech. Appl., vol. 27. Springer.
Hormann, K., Floater, M.S., 2006. Mean value coordinates for arbitrary planar polygons. ACM Trans. Graph. 25 (4), 1424–1441.
Hormann, K., Greiner, G., 2000. MIPS: an efficient global parametrization method. In: Laurent, P.-J., Sablonnière, P., Schumaker, L.L. (Eds.), Curve and Surface Design. Saint-Malo, 1999. Vanderbilt University Press, Nashville, TN, pp. 153–162.
Jacobson, A., Baran, I., Popović, J., Sorkine, O., 2011. Bounded biharmonic weights for real-time deformation. ACM Trans. Graph. 30 (4). Article 78, 8 pp.
Joshi, P., Meyer, M., DeRose, T., Green, B., Sanocki, T., 2007. Harmonic coordinates for character articulation. ACM Trans. Graph. 26 (3). Article 71, 9 pp.
Kanai, T., Suzuki, H., Kimura, F., 1997. 3D geometric metamorphosis based on harmonic map. In: Proceedings of Pacific Graphics. Seoul, pp. 97–104.
Kneser, H., 1926. Lösung der Aufgabe 41. Jahresber. Dtsch. Math.-Ver. 35 (2. Abteilung), 123–124.
Laugesen, S.R., 1996. Injectivity can fail for higher-dimensional harmonic extensions. Complex Var. Theory Appl. 28 (4), 357–369.
Lee, S., Wolberg, G., Shin, S.Y., 1997. Scattered data interpolation with multilevel B-splines. IEEE Trans. Vis. Comput. Graph. 3 (3), 228–244.
Lipman, Y., 2012. Bounded distortion mapping spaces for triangular meshes. ACM Trans. Graph. 31 (4). Article 108, 13 pp.
Lipman, Y., Funkhouser, T., 2009. Möbius voting for surface correspondence. ACM Trans. Graph. 28 (3). Article 72, 12 pp.
Martin, S., Kaufmann, P., Botsch, M., Wicke, M., Gross, M., 2008. Polyhedral finite elements using harmonic basis functions. Comput. Graph. Forum 27 (5), 1521–1529.
Pinkall, U., Polthier, K., 1993. Computing discrete minimal surfaces and their conjugates. Exp. Math. 2 (1), 15–36.
Poranne, R., Lipman, Y., 2014. Provably good planar mappings. ACM Trans. Graph. 33 (4). Article 76, 11 pp.
Radó, T., 1926. Aufgabe 41. Jahresber. Dtsch. Math.-Ver. 35 (2. Abteilung), 49.
Rustamov, R.M., 2007. Boundary element formulation of harmonic coordinates. Tech. rep. Department of Mathematics, Purdue University.
Schneider, T., Hormann, K., Floater, M.S., 2013. Bijective composite mean value mappings. Comput. Graph. Forum 32 (5), 137–146.
Schüller, C., Kavan, L., Panozzo, D., Sorkine-Hornung, O., 2013. Locally injective mappings. Comput. Graph. Forum 32 (5), 125–135.
Sheffer, A., Praun, E., Rose, K., 2006. Mesh parameterization methods and their applications. Found. Trends Comput. Graph. Vis. 2 (2), 105–171.
Sorkine, O., Cohen-Or, D., Goldenthal, R., Lischinski, D., 2002. Bounded-distortion piecewise mesh parameterization. In: Proceedings of IEEE Visualization. Boston, pp. 355–362.
Strang, G., Fix, G., 2008. An Analysis of The Finite Element Method, 2nd edition. Wellesley–Cambridge Press.
Wächter, A., Biegler, L.T., 2006. On the implementation of an interior-point filter line-search algorithm for large-scale nonlinear programming. Math. Program., Ser. A 106 (1), 25–57.
Weber, O., Ben-Chen, M., Gotsman, C., 2009. Complex barycentric coordinates with applications to planar shape deformation. Comput. Graph. Forum 28 (2), 587–597.
Weber, O., Ben-Chen, M., Gotsman, C., Hormann, K., 2011. A complex view of barycentric mappings. Comput. Graph. Forum 30 (5), 1533–1542.
Weber, O., Gotsman, C., 2010. Controllable conformal maps for shape deformation and interpolation. ACM Trans. Graph. 29 (4). Article 78, 11 pp.
Weber, O., Myles, A., Zorin, D., 2012. Computing extremal quasiconformal maps. Comput. Graph. Forum 31 (5), 1679–1689.
Weber, O., Zorin, D., 2014. Locally injective parametrization with arbitrary fixed boundaries. ACM Trans. Graph. 33 (4). Article 75, 12 pp.